Journal of Power Sources 232 (2013) 258–263

Contents lists available at SciVerse ScienceDirect

Journal of Power Sources

journal homepage: www.elsevier.com/locate/jpowsour

Short communication

High capacity Li_2MnSiO_4/C nanocomposite prepared by sol–gel method for lithium-ion batteries

Shuangke Liu*, Jing Xu*, Dezhan Li, Yun Hu, Xiang Liu, Kai Xie

College of Aerospace Science and Engineering, National University of Defense Technology, Changsha 410073, China

HIGHLIGHTS

- A high capacity Li_2MnSiO_4/C nanocomposite was prepared by sol–gel method.
- Amorphous carbon coat on the Li_2MnSiO_4 crystals uniformly.
- The nanocomposite has a high initial discharge capacity and superior rate capacity.
- The high capacity is ascribed to the nanoparticle size and uniform carbon coating.

ARTICLE INFO

Article history:
Received 21 July 2012
Received in revised form
25 October 2012
Accepted 14 December 2012
Available online 17 January 2013

Keywords:
Lithium-ion batteries
Lithium manganese silicate
Carbon-coated
High capacity
Sol–gel

ABSTRACT

A high capacity Li_2MnSiO_4 (LMS)/C nanocomposite has been prepared by glucose assisted sol–gel method with in situ carbon coating. X-ray diffraction (XRD) measurements confirm the formation of orthorhombic structure with $Pmn2_1$ space group. Field emission scanning electron microscopy (FESEM) shows that the LMS/C powders consist of uniformly distributed nanoparticles with size in the range of 20–50 nm and high-resolution transmission electron microscopy (HRTEM) confirms that amorphous carbon coat on the LMS nanocrystals. Electrochemical tests reveal that the LMS/C nanocomposite has a high initial discharge capacity of 253.4 mA h g^{-1} at 10 mA g^{-1} and superior rate capability (193.1 mA h g^{-1} at 160 mA g^{-1} and 149.9 mA h g^{-1} at 320 mA g^{-1}). The improved electrochemical performance is ascribed to coated carbon and nanoparticle size, which can enhance the electronic conductivity as well as lithium-ion diffusion coefficient.

1. Introduction

Lithium ion batteries have been widely used in portable electronic devices due to their high energy density, long cycle life and environmental friendliness [1,2]. However, current commercialized cathode materials in Li-ion batteries, such as $LiCoO_2$, $LiMn_2O_4$, $LiFePO_4$, etc., exhibit limited practical capacity (<200 mA h g^{-1}) because of their intrinsic structure that can only allow one Li^+ or even less than one Li^+ per formula unit to insert into the cathodic host lattice [3–5]. Thus, it is necessary to develop high capacity cathode in order to meet the energy demands of future electric vehicles (EVs) and hybrid electric vehicles (HEVs) [6,7]. The new orthosilicate family of Li_2MSiO_4 (M = Fe, Mn, Co, Ni) has attracted great interest because of their appealing advantages such as high theoretical capacity (330 mA h g^{-1}), high safety and low cost [8–12]. Among this family, Li_2MnSiO_4 (LMS) is much more feasible to achieve two lithium (Mn^{2+}/Mn^{3+} and Mn^{3+}/Mn^{4+}) insertion/extraction than other orthosilicates [12], within the voltage range of current electrolyte system.

However, reports on more than one lithium insertion/extraction for LMS cathode material are scarce [13–15] because of the following reasons: 1) it's difficult to obtain phase-pure LMS material, impurities always appear when either prepared by solid state reaction [16,17] or by sol–gel route [12,13,18–20], and the presence of impurities could greatly worsen the electrochemical performance of the active material; 2) LMS suffers from poor electronic conductivity ($\sim 10^{-16}$ S cm^{-1} at room temperature) [21], which is even five orders of magnitude lower than that of the olivine $LiFePO_4$.

Accordingly, much effort has been made to improve the electrochemical performance of LMS, including particle size tailoring and surface modification. Sol–gel synthesis is one of the most efficient ways to prepare nano-sized particles with high phase purity, and carbon coating is the commonly used way to increase electronic conductivity of the electrode materials. In previous

* Corresponding authors. Fax: +86 (0)731 84576578.
E-mail addresses: liu_sk@139.com (S. Liu), xujin503@163.com (J. Xu).

0378-7753/$ – see front matter © 2013 Elsevier B.V. All rights reserved.
http://dx.doi.org/10.1016/j.jpowsour.2012.12.126

reports, two kinds of carbon coating were employed. One is in-situ carbon coating achieved accompany with the synthesis process, the other is ex-situ carbon coating obtained by post treatment after synthesis. Belharouak et al. [18] reported LMS cathode material synthesized via an all-acetate precursor sol–gel method, but they only obtained an initial discharge capacity of 135 mA h g^{-1} after treatment by carbon coating using cellulose as the carbon source. Yang et al. [13] prepared LMS/C nanocomposite through a solution route, which could deliver a reversible capacity of 209 mA h g^{-1} in the first cycle. Aravindan and co-workers [16] synthesized LMS/C by one-step solid state reaction, the composite obtained delivered an initial discharge capacity of 160 mA h g^{-1} with stable cycling. These studies indicate that the in-situ carbon coating is likely to provide more homogeneous coating layer than ex-situ coating, and hence benefits to improve the electrochemical performance of LMS cathode.

Herein, a glucose assisted sol–gel method with in-situ carbon coating was used to obtain phase-pure and nano-sized LMS/C composite. All starting materials could be dissolved in the mixed solution, and thus a uniform gel was formed, the gel was sintered subsequently to obtain carbon-coated LMS composite. The structure, morphology, physical and electrical properties were investigated by XRD, SEM, conductivity measurements and electrochemical impedance spectroscopy (EIS). It is found that the as-prepared LMS/C composite has a high initial capacity of 253.4 mA h g^{-1} and superior rate capability, possibly serves as a candidate cathode for high capacity lithium-ion batteries.

2. Experimental

2.1. Materials synthesis

The LMS/C nanocomposite was prepared via a sol–gel method using glucose as carbon source. First, 0.02 mol $CH_3COOLi \cdot 2H_2O$ and 0.01 mol $Mn(CH_3COO)_2 \cdot 4H_2O$ (99% purity, Tianjin Damao chemical Reagent Co., Ltd) were dissolved in water–acetic acid solution (3.6 g water and 7.2 g acetic acid), and then 1.0 g glucose (99% purity) was added, dissolved. Subsequently the solution of 0.01 mol $Si(OC_2H_5)_4$ (99% purity, Tianjin Damao chemical Reagent Co., Ltd) and 8 ml isopropanol (99% purity) was added with continuous stirring. The transparent solution was evaporated at 80 °C to enable the formation of gel. After drying the wet gel under 100 °C for 24 h, the dry gel precursor was finely ground and then calcined at 650 °C for 6 h in a flowing nitrogen atmosphere to obtain the LMS/C nanocomposite. The synthesis process of pristine LMS was similar to that of LMS/C without adding glucose.

2.2. Materials characterizations

The structure of pristine LMS and LMS/C nanocomposite was measured by XRD (SIEMENS D-500) using Cu Kα radiation, ranging from 10° to 80° at a step of 6° min^{-1}. The micro morphologies of the composites were studied using field emission scanning electron microscopy (HITACHI S4800, Japan) and transmission electron microscopy (TEM, TECNAI, Philips, Netherlands). The carbon content in the composite was determined by elemental analyzer (Elementar vario EL III, Germany). The electronic conductivity of the nanocomposite was measured by a four-probe meter detector (China, RTS-8) at room temperature.

2.3. Electrochemical characterization

The cathode electrode of the LMS/C nanocomposite was prepared by mixing 80 wt% active material (LMS/C) with 10 wt% Super P and 10 wt% polyvinylidene fluoride (PVDF) binder using N-methyl-pyrrolidone (NMP) as the solvent, while the electrode of the pristine LMS was prepared by mixing 70 wt% active material (LMS) with 20 wt% Super P and 10 wt% PVDF binder. After mixing well, the slurry was pasted on aluminum foil and dried overnight at 100 °C in a vacuum oven. The average loading was ~1.5 mg cm^{-2}. The metallic lithium foils and 1 M $LiPF_6$ diethyl carbonate/ethylene carbonate (1:1 by volume) were used as the anode and electrolyte, respectively, and Celgard 2400 was the separator. Galvanostatic charge/discharge measurements were performed using a battery tester (LAND CT-2001A, Wuhan, China) at room temperature in a potential range of 1.5–4.8 V (vs. Li^+/Li) at various current densities. The specific capacity was calculated based on the mass of LMS, excluding the coated carbon and Super P. Electrochemical impedance experiments were conducted using an electrochemical work station (CHI660D, Chenhua Ltd Co., Shanghai, China) with Li foil as both counter and reference electrodes. The amplitude of AC perturbation signal was 5 mV and the frequency range was from 10^5 to 10^{-1} Hz. The EIS data were analyzed using Zview software.

3. Results and discussion

3.1. XRD, SEM and TEM analysis

Fig. 1 shows the powder X-ray diffraction patterns of the synthesized pristine LMS and LMS/C nanocomposite at 650 °C. As is seen, the diffraction patterns of both LMS and LMS/C can be indexed to the orthorhombic $Pmn2_1$ structure, which is in good agreement with the calculated LMS patterns [22]. Compared to the XRD pattern of LMS, the diffraction peaks of the LMS/C nanocomposite appeared much weaker and broader, indicating that the presence of carbon could prevent the growth and aggregation of the LMS grains, and thus lead to a decrease in crystallite size. In addition, apart from the standard peaks of LMS, three other inconspicuous peaks located at 19.5°, 30.7°, 35.0° and 40.7° can be observed in the XRD pattern of the LMS, which can be attributed to the Li_2SiO_3, Mn_2SiO_4 and MnO impurities. Those impurities were also detected in previous reports [13,16–20,22]. However, in the XRD pattern of LMS/C, no impurities were observed, implying that the adding of glucose in the synthesis process could prevent the generation of impurities during calcination.

Morphological features of the pristine LMS and LMS/C nanocomposite are shown in Fig. 2a and b. It can be observed that the pristine LMS (Fig. 2a) consists of irregular congregated particles with

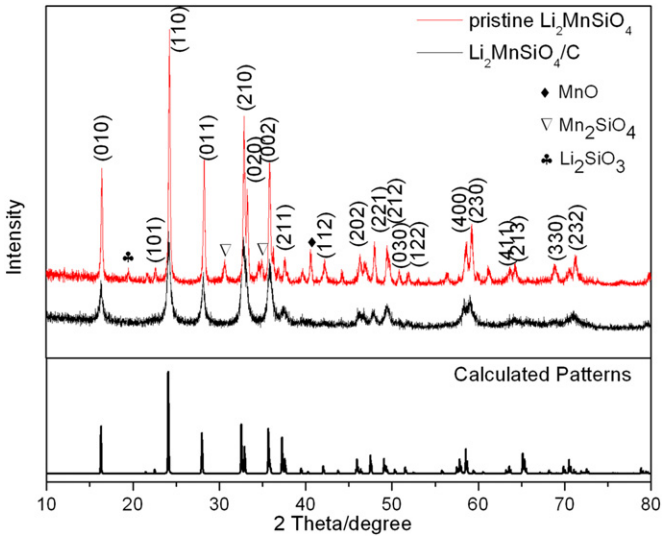

Fig. 1. XRD patterns of the pristine LMS and the LMS/C nanocomposite.

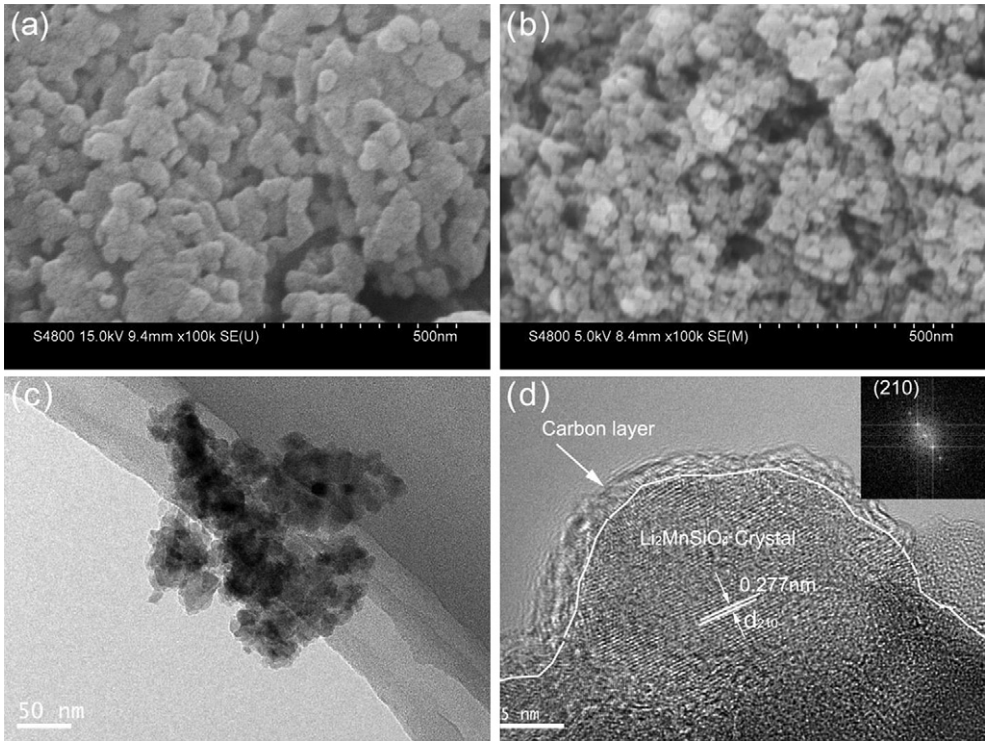

Fig. 2. FESEM images of (a) the pristine LMS and (b) the LMS/C nanocomposite, (c) TEM and (d) HRTEM images of the LMS/C nanocomposite.

size of 50–100 nm while the LMS/C nanocomposite (Fig. 2b) exhibits uniformly distributed particle size ranging from 20 to 50 nm, further demonstrating that the adding of glucose into the precursor solution could decrease the particle size. The LMS/C nanocomposite is selected for further investigation by TEM and HRTEM. It can be clearly seen from the TEM image in Fig. 2c that the LMS/C particles have uniform size distribution of 20–50 nm with spherical morphology, which is in good agreement with the FESEM image (Fig. 2b). Fig. 2d shows the HRTEM image of the LMS/C nanocomposite. The entire LMS particle is coated by rather uniform layer of amorphous carbon with a thickness of 2–3 nm. The legible lattice fringe with basal distance of 0.277 nm can also be observed in Fig. 2d, which is consistent with the (210) lattice spacing of orthorhombic Li_2MnSiO_4. This is further validated by the corresponding selected-area electron diffraction (SAED) pattern (inset). Therefore, it is expected that the LMS/C with nanoparticle size and uniform carbon coating may provide short pathways and huge electrochemical interfaces for fast ions diffusion and transportation.

3.2. Conductivity measurements

The carbon content in the pristine LMS and LMS/C nanocomposite is determined to be 0.29 and 9.88 wt%, respectively. The electronic conductivity of the LMS/C nanocomposite is measured to be 5.13×10^{-3} S cm^{-1} while that is too low to be measured for the pristine LMS. Nevertheless, compared to the reported value of LMS ($\sim 10^{-16}$ S cm^{-1} at room temperature), the electronic conductivity of the LMS/C nanocomposite in this work is far higher by over ten orders of magnitude, which indicates the in situ carbon coating could largely enhance the electronic conductivity.

3.3. Electrochemical performance

The electrochemical performance of the pristine LMS and LMS/C composite is evaluated in the Li/LMS cell configuration in the voltage range of 1.5–4.8 V at room temperature. Fig. 3a and b shows typical charge/discharge profiles of the two electrodes at a current density of 10 mA g^{-1}.

The discharge capacity of the LMS/C nanocomposite in the first cycle is 253.4 mA h g^{-1} while it is only 47.9 mA h g^{-1} for the pristine LMS. Although the content of Super P is 20 wt% for the pristine LMS electrode, which is equal to the total content of coated carbon (9.88 wt%) and Super P (10 wt%) for the LMS/C electrode, the discharge capacity of the pristine LMS electrode is still much lower than that of the LMS/C electrode. This comparison demonstrates that the in situ carbon coating is more efficient to improve the electrochemical performance of LMS than the post Super P adding during cell fabrication. Besides, the impurities (Li_2SiO_3, Mn_2SiO_4 and MnO) in pristine LMS might be another cause which leads to the poor electrochemical performance of the material, possibly due to the instable domains of the impurity phases [18].

The high discharge capacity of 253.4 mA h g^{-1} obtained for the LMS/C nanocomposite indicates more than one electron (1.53 Li^+) transfer during the intercalation/deintercalation process, corresponding to 77% of its theoretical two-electron redox capacity (330 mA h g^{-1}). Although using a similar loading density of active material as ours when making electrodes, Dominko's [23] and Ghosh's groups [24] obtained initial capacity of only $\sim$100 mA h g^{-1} and 161 mA h g^{-1}, respectively, values which are inferior to our results.

Fig. 4 shows the dQ/dV vs. voltage plots of the LMS/C, two cathodic peaks located at 4.2 V and 4.65 V during first charge may be attributed to the Mn^{2+}/Mn^{3+} and Mn^{3+}/Mn^{4+} redox couples, respectively. But during first discharge, it shows only one inconspicuous anodic peak at 2.9 V, which indicates the low reversibility of the cathode material. In addition, the redox peaks of the LMS/C material tend to disappear during the second charge, which may be due to the structural rearrangements during the first cycle.

To fully estimate the electrochemical performance of the LMS/C cathode, galvanostatic cycling measurement was also performed at different current densities. As can be seen in Fig. 5a, the initial discharge capacity of LMS/C is 216.3, 193.1 and 149.9 mA h g^{-1} at 80,

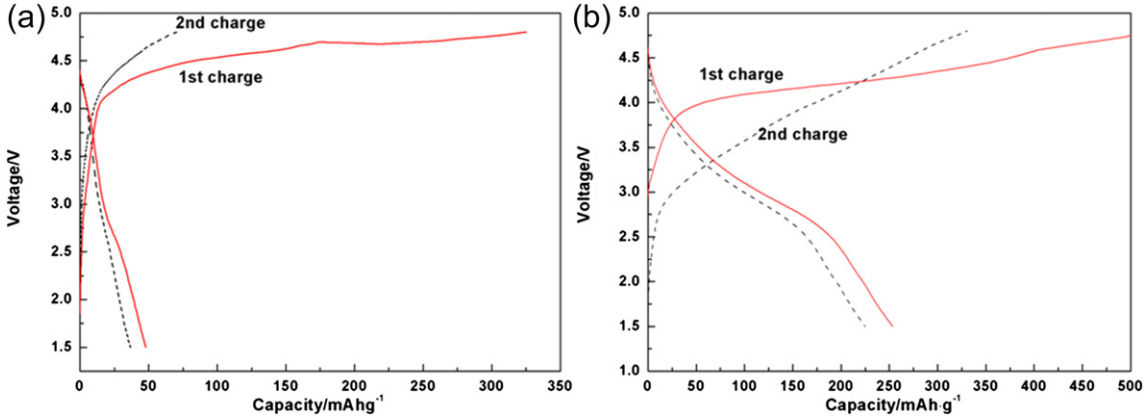

Fig. 3. Charge/discharge profiles of (a) the pristine LMS and (b) the LMS/C nanocomposite at 10 mA g^{-1}.

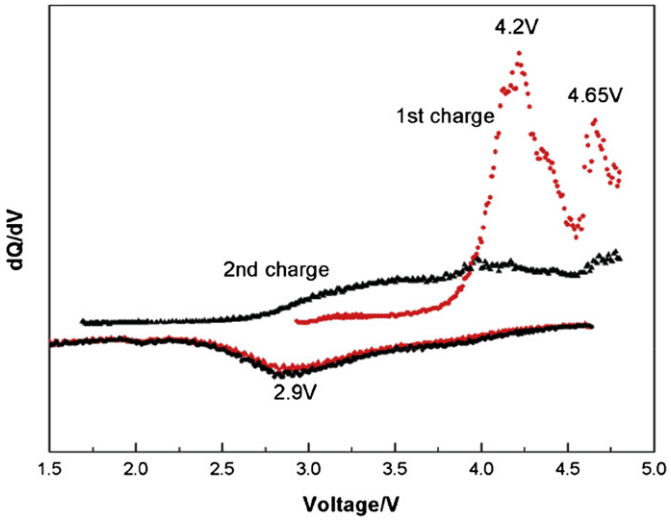

Fig. 4. d*Q*/d*V* vs. voltage plots of LMS/C nanocomposite at 10 mA g^{-1}.

160 and 320 mA g^{-1}, respectively. Although the LMS cathode material suffers from extremely low electronic conductivity and was reported having very poor rate capacity before, our results indicate that the rate performance of LMS can be largely improved by carbon coating. Table 1 exhibits that, in comparison to the previously reported LMS, our LMS/C nanocomposites have much better rate performance which can be ascribed to the great enhancement of the electronic conductivity by in situ carbon coating. However, the LMS/C nanocomposites still suffer from severe capacity fading, only 44%, 46.8% and 56.4% capacity retentions were obtained at 80, 160 and 320 mA g^{-1} after 20 cycles. The capacity fade may be associated with the amorphous tendency during electrochemical cycling [13], the manganese dissolution and Jahn–Teller effect of Mn^{3+} which caused the volumetric effect and destroyed the structure of the materials [14].

3.4. EIS analysis

In order to further identify the kinetic properties of the pristine LMS and the LMS/C nanocomposite, EIS measurements of both electrodes were conducted and presented in Fig. 6. The equivalent circuit model [24] used for fitting these impedance data is shown in the inset of Fig. 6a. Both EIS spectrums are composed of a semicircle

Table 1
Comparison of the rate capability of the LMS/C nanocomposite in this work with those reported in some previous literature.

	Discharge capacity (mA h g^{-1})	Reference
This work	253.4 (10 mA g^{-1}), 149.9 (320 mA g^{-1})	
Li et al.	209 (5 mA g^{-1}), 135 (150 mA g^{-1})	[13]
Muraliganth et al.	210 (C/20), 133 (1 C)	[14]

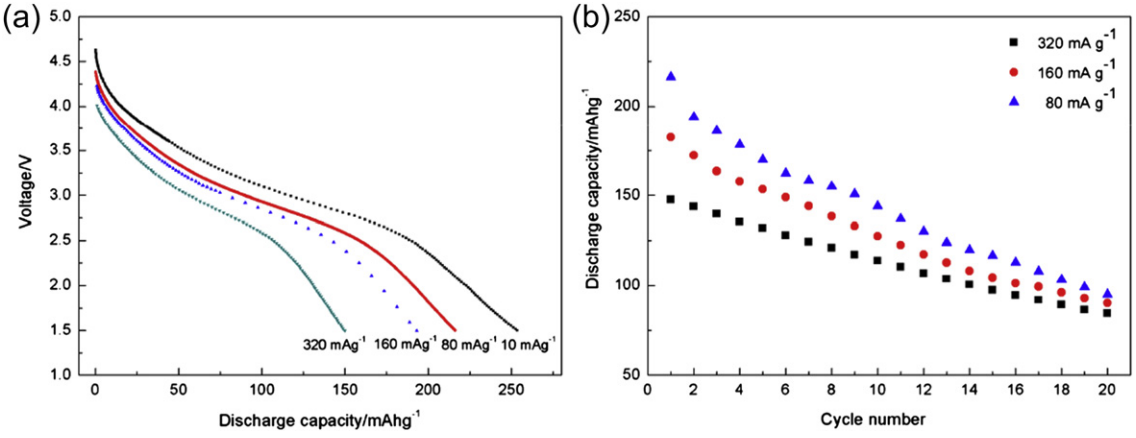

Fig. 5. (a) Discharge profiles and (b) cycling performance of the LMS/C nanocomposite at different current densities.

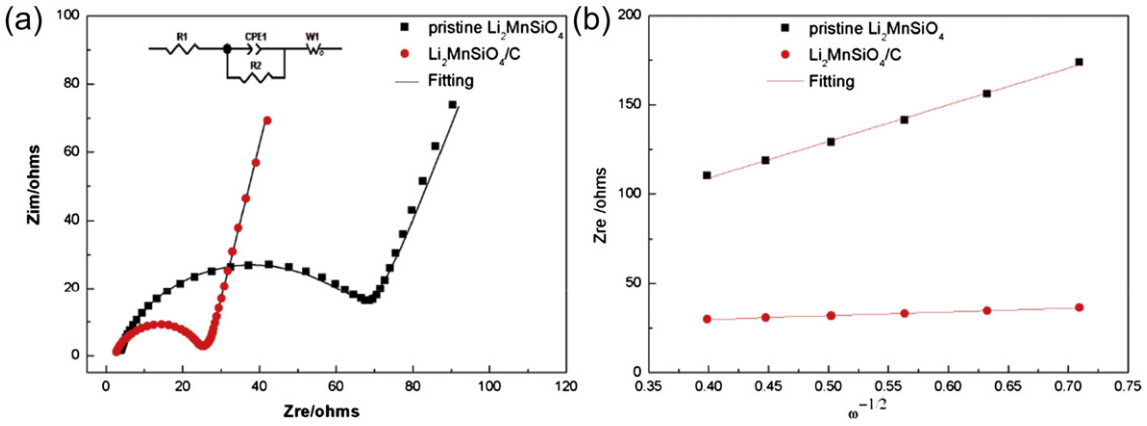

Fig. 6. (a) Nyquist plot of the pristine LMS and LMS/C nanocomposite electrodes and (b) linear relationship between Z_{re} and $\omega^{-1/2}$ in the low frequency region.

at the high to medium frequency region and an inclined line in the low frequency range. An intercept along the Z_{re} axis at high frequency zone corresponds to the ohmic resistance (R_e), which represents the resistance of the electrolyte. The semicircle in the middle frequency range is attributed to the charge transfer process, whose diameter on the Z_{re} axis is approximately equal to the charge transfer resistance (R_{ct}). The inclined line is attributed to the diffusion of the lithium ions into the bulk of the active material, which are called Warburg diffusion (Z_w). All the parameters obtained from EIS simulations are recorded in Table 2. It could be seen that the diameter of the semicircle in the medium-frequency range for the LMS/C nanocomposite electrode is much smaller than that of the pristine LMS, indicating that the electronic conductivity of the LMS/C was dramatically improved after in situ carbon coating. The Warburg coefficient σ_w can be obtained by Eq. (1):

$$Z_{re} = R_e + R_{ct} + \sigma_w \omega^{-1/2} \quad (1)$$

where ω ($2\pi f$) is the angular frequency in the low frequency region, both R_e and R_{ct} are kinetics parameters independent of frequency. Therefore, Z_{re} has a linear relationship with $\sigma_w^{-1/2}$ (Fig. 6b), while the slope of the fitting line represents σ_w. Consequently, using the resulting σ_w, the diffusion coefficient of the lithium ions (D_{Li^+}) can be calculated based on Eq. (2) [25]:

$$D_{Li^+} = \frac{R^2T^2}{2A^2n^4F^4C^2\sigma_w^2} \quad (2)$$

In this equation, R is the gas constant (8.314 J mol^{-1} K^{-1}), T is the temperature (298.5 K), A is the area of the electrode (2.5434 cm^2 in this study), F is the Faraday's constant (96,500 C mol^{-1}) and C is the molar concentration of Li ions (0.0195 mol cm^{-3}).

Table 2 presents the calculated lithium ion diffusion coefficient for the pristine LMS and the LMS/C nanocomposite. It can be observed that the coefficient was 3.34×10^{-14} cm^2 s^{-1} for the LMS/C nanocomposite, which is two orders of magnitude higher than that of the pristine LMS. The above results substantially indicate that the in situ carbon coating could efficiently enhance the lithium ions diffusion coefficient, and thus lead to an improvement of electrochemical performance.

Table 2
Impedance parameters of the pristine LMS and the LMS/C nanocomposite.

	R_e (Ω)	R_{ct} (Ω)	σ_w (Ω cm^2 s$^{-1/2}$)	D_{Li^+} (cm^2 s^{-1})
LMS/C	2.4	22.6	20.80	3.34×10^{-14}
LMS	3.22	62.55	205.31	3.42×10^{-16}

4. Conclusions

To conclude, a high capacity LMS/C nanocomposite has been prepared by a glucose assisted sol–gel method with in situ carbon coating. XRD and TEM characterizations show that the presence of carbon could prevent the formation of impurities and the growth of particle size. The as-prepared LMS/C nanocomposite has a high initial discharge capacity of 253.4 mA h g^{-1} and superior rate capacity. The improved electrochemical performance is ascribed to the nanoparticle size and uniform carbon coating, which can enhance the electronic conductivity as well as lithium ion diffusion coefficient.

Acknowledgments

This work was financially supported by the Aid Program for Science and Technology Innovative Research Team in Higher Educational Institutions of Hunan Province.

References

[1] B. Dunn, H. Kamath, J.M. Tarascon, Science 334 (2011) 928–935.
[2] J. Liu, J.G. Zhang, Z.G. Yang, J.P. Lemmon, C. Imhoff, G.L. Graff, L.Y. Li, J.Z. Hu, Z.M. Wang, J. Xiao, G. Xia, V.V. Viswanathan, S. Baskaran, V. Sprenkle, X.L. Li, Y.Y. Shao, B. Schwenzer, Adv. Funct. Mater. (2012). http://dx.doi.org/10.1002/adfm.201200690.
[3] M. Armand, J.M. Tarascon, Nature 451 (2008) 652–657.
[4] X.P. Gao, H.X. Yang, Energy Environ. Sci. 3 (2010) 174–189.
[5] Z.X. Chen, S. Qiu, Y.L. Cao, X.P. Ai, K. Xie, X.B. Hong, H.X. Yang, J. Mater. Chem. 22 (2012) 17768–17772.
[6] M.S. Whittingham, Chem. Rev. 104 (2004) 4271–4302.
[7] A. Manthiram, J. Phys. Chem. Lett. 2 (2011) 176–184.
[8] A. Nyten, A. Abouimrane, M. Armand, T. Gustafsson, J.O. Thomas, Electrochem. Commun. 7 (2005) 156–160.
[9] M.E.A. de Dompablo, M. Armand, J.M. Tarascon, U. Amador, Electrochem. Commun. 8 (2006) 1292–1298.
[10] R. Dominko, J. Power Sources 184 (2008) 462–468.
[11] M.S. Islam, R. Dominko, C. Masquelier, C. Sirisopanaporn, A.R. Armstrong, P.G. Bruce, J. Mater. Chem. 21 (2011) 9811–9818.
[12] R. Dominko, M. Bele, A. Kokalj, M. Gaberscek, J. Jamnik, J. Power Sources 174 (2007) 457–461.
[13] Y.X. Li, Z.L. Gong, Y. Yang, J. Power Sources 174 (2007) 528–532.
[14] T. Muraliganth, K.R. Stroukoff, A. Manthiram, Chem. Mater. 22 (2010) 5754–5761.
[15] D.M. Kempaiah, D. Rangappa, I. Honma, Chem. Commun. 48 (2012) 2698–2700.
[16] V. Aravindan, K. Karthikeyan, S. Ravi, S. Amaresh, W.S. Kim, Y.S. Lee, J. Mater. Chem. 21 (2011) 2470–2475.
[17] K. Gao, C.S. Dai, J. Lv, S.D. Li, J. Power Sources 211 (2012) 97–102.

[18] I. Belharouak, A. Abouimrane, K. Amine, J. Phys. Chem. C 113 (2009) 20733–20737.
[19] C. Deng, S. Zhang, B.L. Fu, S.Y. Yang, L. Ma, Mater. Chem. Phys. 120 (2010) 14–17.
[20] Q.Q. Zhang, Q.C. Zhuang, S.D. Xu, X.Y. Qiu, Y.L. Cui, Y.L. Shi, Y.H. Qiang, Ionics 18 (2012) 487–494.
[21] A. Kokalj, R. Dominko, G. Mali, Chem. Mater. 19 (2007) 3633–3640.
[22] M.E.A. de Dompablo, R. Dominko, J.M.G. Amores, L. Dupont, G. Mali, H. Ehrenberg, J. Jamnik, E. Morán, Chem. Mater. 20 (2008) 5574–5584.
[23] R. Dominko, M. Bele, M. Gaberscek, A. Meden, M. Remskar, J. Jamnik, Electrochem. Commun. 8 (2006) 217–222.
[24] P. Ghosh, S. Mahanty, R.N. Basu, J. Electrochem. Soc. 156 (2009) A677–A681.
[25] A.J. Bard, J.R. Faulkner, Electrochemical Methods, second ed., Wiley, 2001, p. 231.